Excimer laser photoablation of silicon

G. B. Shinn, F. Steigerwald, H. Stiegler, R. Sauerbrey, F. K. Tittel, and W. L. Wilson, Jr.
Department of Electrical and Computer Engineering and Rice Quantum Institute, Rice University, Houston, Texas 77251

(Received 9 May 1986; accepted 21 July 1986)

The ultraviolet and visible emission spectra from excimer laser-produced silicon plasmas were studied and the ablation rate measured as a function of laser energy density and wavelength. A spectroscopic investigation of the laser-produced plasma showed Si I, Si II, and Si III spectral lines with higher laser intensity causing a higher degree of ionization in the plasma. Both time-integrated and time-resolved spectroscopic studies showed electronic transitions superimposed on a weak continuum over the entire range from 250 to 640 nm. The photoablation rate of Si was independent of laser wavelength (193 or 248 nm), and had an energy density threshold of ≈ 1.3 J/cm^2. The threshold was almost independent of the buffer gas pressure between vacuum and 1000 Torr. These results are described in the framework recently developed for excimer laser ablation of metals.

I. INTRODUCTION

The use of laser radiation for processing semiconductor materials has recently received much attention.[1,2] In particular, the widespread availability of commercial excimer lasers has made this technique a promising area of development. Excimer lasers possess a number of characteristics, such as high power and multiple available wavelengths in the ultraviolet, which are ideal for such processing applications. Thus, the potential exists to drive photochemical reactions at useful rates using the high power of an excimer laser while selectively driving the desired process by suitable choice of wavelength. During laser-driven deposition or etching of materials on a semiconductor as well as with laser annealing, however, laser radiation may be absorbed by the underlying semiconductor material. Information concerning the threshold at which damage occurs and a means to detect when damage begins to occur are necessary to determine limits on laser intensity and wavelength for safe laser-assisted processing. Understanding the interaction of intense laser radiation with the semiconductor substrate is therefore very important. In this work we present a study of the excimer laser ablation process of silicon. The silicon plasma plume which was formed by high intensity 193 nm ArF and 248 nm KrF radiation was studied spectroscopically. A similar spectroscopic study of laser-produced carbon plasma plumes was recently published by Koren and Yeh.[3] The rate of silicon ablation was measured as a function of pulse energy, and the energy threshold for damage was determined.

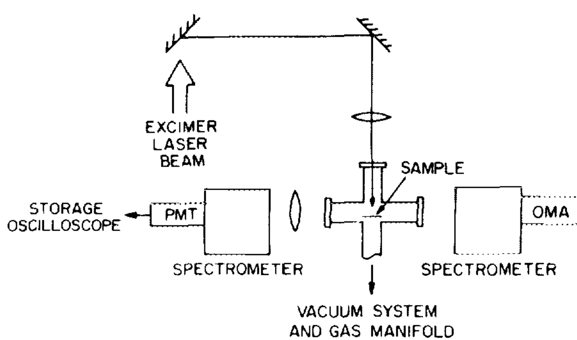

FIG. 1. Schematic drawing of experimental apparatus.

II. EXPERIMENTAL APPARATUS

The cell in which the investigation was performed was constructed from a commercial stainless steel tubing cross (Fig. 1). The upper flange of the cell was fitted with a MgF_2 window through which the excimer laser radiation passed. Sapphire windows on the side flanges were used for visual observation and spectroscopic measurements. The remaining flange was connected to a gas system and diffusion vacuum pump. A stainless steel sample holder supported the silicon sample in the center of the cell perpendicular to the laser beam.

The laser source was a Lambda Physik EMG-101 excimer laser operated at either the ArF 193 nm wavelength or the KrF 248 nm wavelength. The laser pulse length was approximately 18 ns for KrF and about 14 ns for ArF, and pulse repetition rates from 1 to 5 Hz were used. The laser energy varied between 20 and 200 mJ per pulse, as measured with a Gentec ED-500 calorimeter. The beam was directed into the cell by two turning mirrors. MgF_2-coated aluminum mirrors were used at 248 nm, and dielectric mirrors were used at 193 nm. The beam was focused onto the sample with a spherical calcium fluoride lens having a focal length of 15 cm. A rectangular mask was used over the cell window in order to admit only the central, uniform portion of the laser beam.

The sample material was *p*-type (100) silicon. The samples were cut from 3 in. diam wafers with a thickness of 0.460 mm and resistivity of 10–20 Ω cm. Before each experiment, the cell was pumped out to less than 5×10^{-5} Torr and refilled with helium (1000 Torr in most cases) in order to prevent deposition of silicon vapor on the cell windows.

Each pulse of the focused laser beam produced a bright plasma plume above the silicon sample. Spectroscopic observations of this emission were made by directing light from the plume above the sample to two spectrometers, equipped with either a photomultiplier tube (PMT) or an optical multichannel analyzer (OMA). A Jarrell-Ash 1/4 m spectrom-

 © 1986 American Vacuum Society

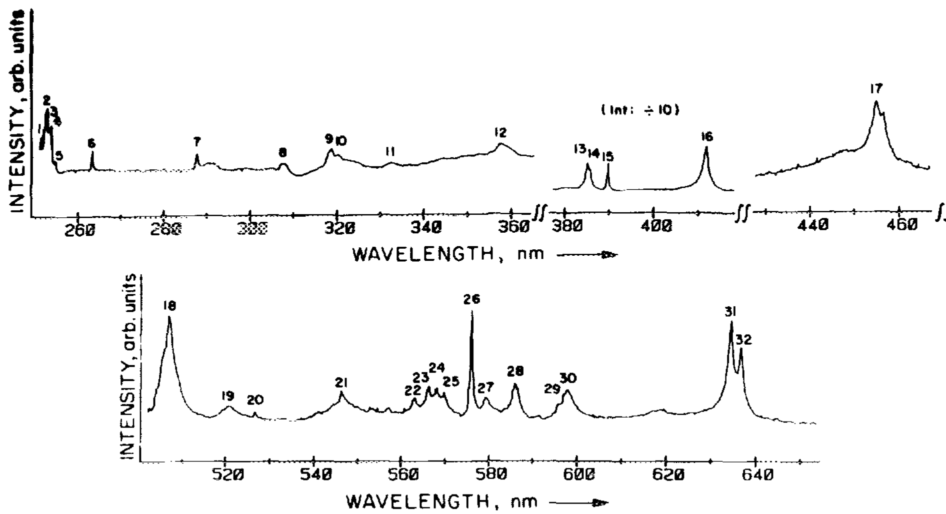

FIG. 2. Time-integrated emission spectrum from KrF excimer laser-produced silicon plasma. The spectrum between 380 and 415 nm is shown with an intensity scale reduced by a factor of 10. The second order of the 248 nm KrF laser pulse was omitted, and stray light from the visible, which appeared in the range from 260 to 300 nm, was subtracted. No corrections were made for the spectral response of the spectrometer or the OMA detector.

eter was coupled to the PAR OMA-I for observation of time-integrated spectra with a resolution of approximately 0.5 nm. For time resolved measurements, the spectrometer was coupled to an RCA 8575 PMT (3 ns rise time), and an image of the plasma plume was focused onto the entrance slit by a quartz lens of 50 mm focal length. The signal from the PMT was recorded on a Tektronix 7834 storage oscilloscope.

III. RESULTS AND DISCUSSION

A. Spectroscopic analysis of the laser-produced silicon plasma

Power densities on the order of 10^8 W/cm^2 were attained with the focused excimer laser beam and were sufficient to produce a silicon plasma above the wafer. The emission spectrum from this plasma was examined over the range from 250 to 640 nm and shows emissions from neutral silicon Si^+ and Si^{++} (Si I, Si II, and Si III, respectively). A typical time-integrated emission spectrum from a KrF-laser-produced plasma is shown in Fig. 2. The lines originating from singly and doubly ionized silicon are considerably broader than those from the neutral species. The observed emission lines are numbered starting from the lower wavelengths, each corresponding to the wavelengths and transitions listed in Table I. Assignment of the lines was made according to the table of spectral lines found in Ref. 4.

The width of the Si II and Si III lines are much larger than the spectrometer resolution. In the dense plasma above the surface this broadening may be caused either by the plasma electrons or by pressure broadening. If Stark broadening were the dominant broadening mechanism, electron densities of $0.9\text{–}1.8\times10^{18}$ cm^{-3} can be estimated.[5] The same width would be generated by gas densities of $3\text{–}6\times10^{21}$ cm^{-3} corresponding to pressures of several hundred atmospheres.

The emission spectrum of a Si plasma resulting from ArF radiation was studied over the same range as above. However, the less intense of the Si II and Si III emissions were not detected with the ArF laser irradiation due to the lower energy density of the incident beam.

Time-integrated emissions of Si I (390.55 nm), Si II (385.6/386.2 nm), and Si III (455.26 nm) lines were measured at three energy densities of the incident KrF radiation

TABLE I. Silicon species detected in time-integrated emission spectrum from KrF excimer laser-produced plasma (see Fig. 1).

Peak No.	Wavelength (nm)	Species	Transition
1	251.61	Si I	$3p^2\,{}^3P\text{–}4s\,{}^3p^0$ 2–2
	251.43	Si I	$3p^2\,{}^3P\text{–}4s\,{}^3p^0$ 0–1
2	252.41	Si I	$3p^2\,{}^3P\text{–}4s\,{}^3p^0$ 1–0
3	252.85	Si I	$3p^2\,{}^3P\text{–}4s\,{}^3p^0$ 2–1
4	253.24	Si I	$3p^2\,{}^1S\text{–}5s\,{}^1p^0$ 0–1
5	254.18	Si III	$3p\,{}^1P^0\text{–}3p^2\,{}^1D$ 1–2
6	263.56	Si I	$3p^2\,{}^1S\text{–}3d\,{}^1P^0$ 0–1
7	288.16	Si I	$3p^2\,{}^1D\text{–}4s\,{}^1P^0$ 2–1
8	308.62	Si III	$3d\,{}^3D\text{–}4p\,{}^3P^0$ 3–2
	309.34	Si III	$3d\,{}^3D\text{–}4p\,{}^3P^0$ 2–1
	309.68	Si III	$3d\,{}^3D\text{–}4p\,{}^3P^0$ 1–0
9	319.95	Si II	$3d'\,{}^4D^0\text{–}4f'\,{}^4F\,\frac{7}{2}\text{–}\frac{9}{2}$
10	321.00	Si II	$4p\,{}^2P^0\text{–}5d\,{}^2D\,\frac{3}{2}\text{–}\frac{5}{2}$
11	333.31	Si II	$4p\,{}^2P^0\text{–}6s\,{}^2S\,\frac{1}{2}\text{–}\frac{1}{2}$
	333.98	Si II	$4p\,{}^2P^0\text{–}6s\,{}^2S\,\frac{3}{2}\text{–}\frac{1}{2}$
12	359.05	Si III	$4p\,{}^1P^0\text{–}4d\,{}^1D$ 1–2
13	385.60	Si II	$3p^2\,{}^2D\text{–}4p\,{}^2P^0\,\frac{5}{2}\text{–}\frac{3}{2}$
14	386.26	Si II	$3p^2\,{}^2D\text{–}4p\,{}^2P^0\,\frac{3}{2}\text{–}\frac{1}{2}$
15	390.55	Si I	$3p^2\,{}^1S\text{–}4s\,{}^1P^0$ 0–1
16	412.81	Si II	$3d\,{}^2D\text{–}4f\,{}^2F^0\,\frac{3}{2}\text{–}\frac{5}{2}$
	413.09	Si II	$3d\,{}^2D\text{–}4f\,{}^2F^0\,\frac{5}{2}\text{–}\frac{7}{2}$
17	455.26	Si III	$4s\,{}^3S\text{–}4p\,{}^3P^0$ 1–2
	456.78	Si III	$4s\,{}^3S\text{–}4p\,{}^3P^0$ 1–1
	457.48	Si III	$4s\,{}^3S\text{–}4p\,{}^3P^0$ 1–0
18	505.60	Si II	$4p\,{}^2P^0\text{–}4d\,{}^2D\,\frac{3}{2}\text{–}\frac{5}{2}$
	504.10	Si II	$4p\,{}^2P^0\text{–}4d\,{}^2D\,\frac{1}{2}\text{–}\frac{3}{2}$
19	520.24	Si II	$4p'\,{}^4D\text{–}4d'\,{}^4F^0\,\frac{7}{2}\text{–}\frac{9}{2}$
20	527.12	Si I	(2nd order, 263.56 nm)
21	546.64	Si II	$4d\,{}^2D\text{–}6f\,{}^2F^0\,\frac{3}{2}\text{–}\frac{5}{2}$
	546.69	Si II	$4d\,{}^2D\text{–}6f\,{}^2F^0\,\frac{5}{2}\text{–}\frac{7}{2}$
22	563.95	Si II	$4s'\,{}^4P^0\text{–}4p'\,{}^4S\,\frac{5}{2}\text{–}\frac{3}{2}$
23	566.96	Si II	$3d'\,{}^4F^0\text{–}4p'\,{}^4D\,\frac{9}{2}\text{–}\frac{7}{2}$
24	568.88	Si II	$3d'\,{}^4F^0\text{–}4p'\,{}^4D\,\frac{7}{2}\text{–}\frac{5}{2}$
25	570.14	Si II	$3d'\,{}^4F^0\text{–}4p'\,{}^4D\,\frac{5}{2}\text{–}\frac{3}{2}$
26	576.32	Si I	(2nd order, 288.16 nm)
27	580.67	Si II	$4s'\,{}^4P^0\text{–}4p'\,{}^4P\,\frac{1}{2}\text{–}\frac{3}{2}$
28	586.84	Si II	$4s'\,{}^4P^0\text{–}4p'\,{}^4P\,\frac{5}{2}\text{–}\frac{5}{2}$
29	595.76	Si II	$4p\,{}^2P^0\text{–}5s\,{}^2S\,\frac{1}{2}\text{–}\frac{1}{2}$
30	597.90	Si II	$4p\,{}^2P^0\text{–}5s\,{}^2S\,\frac{3}{2}\text{–}\frac{1}{2}$
31	634.71	Si II	$4s\,{}^2S\text{–}4p\,{}^2P^0\,\frac{1}{2}\text{–}\frac{3}{2}$
32	637.14	Si II	$4s\,{}^2S\text{–}4p\,{}^2P^0\,\frac{1}{2}\text{–}\frac{1}{2}$

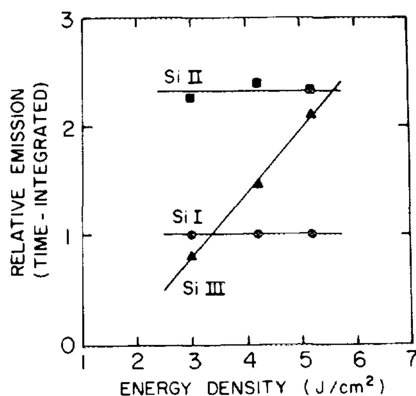

FIG. 3. Ratio of the time-integrated emission from Si II and Si III states (385.6/386.2 and 455.26 nm, respectively) to the emission from the 390.55 nm Si I state as a function of incident KrF laser energy density.

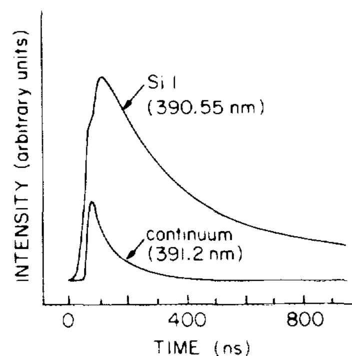

FIG. 4. Temporal evolution of the continuum and line emission from the KrF excimer laser-produced silicon plasma; Si I emission at 390.55 nm and continuum at 391.2 nm.

and normalized to the intensity of the Si I emission at each point (Fig. 3). The overall emission from all silicon species increased with increasing laser energy density. The ratio of the emission from the Si II species to that from the Si I species remained approximately constant over the range from 3 to 5.2 J/cm^2, while the ratio of the emission from the Si III to Si I species increased linearly with energy density. Since the Si I emission has approximately the same laser power density dependence as the singly ionized species, the formation of this Si I species is most likely due to recombination. The actual dynamics of the laser-produced plasma are very complicated. However, the relatively weak power dependence of the Si III emission indicates that the population of this Si III level is through electron impact excitation as well as through multiphoton processes.

Time-resolved spectroscopic studies were performed using a photomultiplier to examine the temporal evolution of species in the laser-induced plasma. Electronic transitions were observed to be superimposed over a weak continuum which covered the entire range from 250 to 640 nm. The continuum was also observed in the time-integrated spectra. The temporal evolution of the Si I emission at 390.55 nm, originating from the $4s\ ^1P^0$ state, and the continuum is shown in Fig. 4. The radiative lifetime of the Si I ($4s\ ^1P^0$) state is 69 ns,[6] whereas the decay constant under our experimental conditions was $\approx$420 ns. The decay time for the Si II emissions at 413 nm was only $\approx$50 ns under the same conditions. These observations indicate that the depopulation of the excited Si I level is governed by the formation of long-lived precursors.

B. Morphology

A SEM micrograph of a representative damage area on Si is shown in Fig. 5. This figure shows the damage crater that was formed after 360 pulses from an ArF laser at a repetition rate of 2 Hz with an energy density of 4 J/cm^2. The nearly rectangular crater has a melt pattern along the bottom which contains ripples that appear to have resolidified as they were propagating outwards from the center along the longer dimension of the crater toward the ends. These ripples have a 15–20 μm periodicity.

It is apparent from Fig. 5 that not all of the irradiated area is ablated uniformly. Typically the sides of the ablated hole parallel to the longer axis are steeper and better defined, whereas the edges of the hole along the shorter dimension have a more gradual slope. The edges of the hole extend slightly above the surrounding wafer, with the center of the hole representing the deepest region. The region around the hole has been lightly cleaned by the laser pulse and exhibits some melting near the ablated region. Qualitative analysis of the sample was done using an energy dispersive spectrometer in the SEM apparatus. The white line surrounding the "cleaned" area is made of fine Si particles, and the debris concentrated along the center of the longer dimension outside of the irradiated spot is composed of larger 1–10 μm Si particles. The debris is round and smooth, and appears as if it has resolidified from liquid droplets.

C. Silicon ablation rate versus incident laser energy density

The ablation rate of Si was measured as a function of incident laser energy density for both KrF and ArF excimer radiation. The energy density of the incident laser pulse was carefully determined. The laser spot size for the ArF laser was $\approx 0.32\ mm^2$ when a mask 3×10 mm was used, and

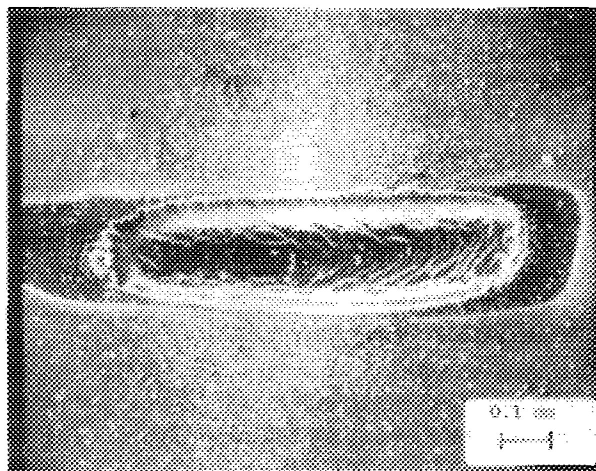

FIG. 5. SEM micrograph of silicon after irradiation by 360 pulses of a focused ArF excimer laser beam at 2 Hz and an energy density of 4 J/cm^2.

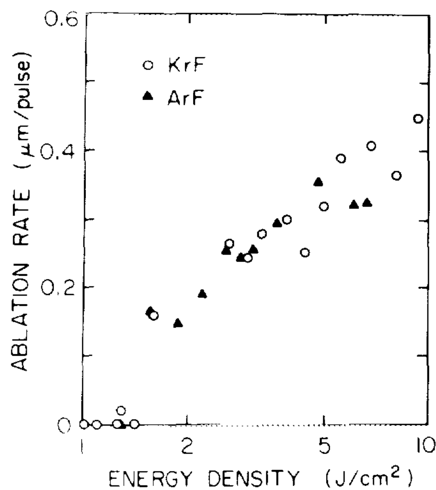

FIG. 6. Silicon ablation rate (μm/pulse) vs the logarithm of the energy density (J/cm^2) of the incident excimer laser beam.

≈ 0.3 mm^2 for the KrF laser using a mask with a 4×15 mm aperture. The total energy delivered to the wafer was measured directly with an energy meter, and an average energy density was calculated. The ablation rate was determined by measuring the depth of the ablated hole using an optical microscope and then dividing by the number of pulses that irradiated the spot. Depth measurements were reproducible to within ± 13 μm, with typical hole depths of 150 μm.

A plot of the logarithm of ablation rate versus the laser energy density is given in Fig. 6. The ablation rate and the ablation threshold are independent of the laser wavelength over this wavelength range, as shown by the fact that the data for both ArF (193 nm) and KrF (248 nm) agree very well over the range from 1.5 to 6 J/cm^2. The linear absorption coefficient of Si does not change significantly between 193 and 248 nm.[7] Therefore our results indicate that excimer laser ablation of silicon close to threshold is largely governed by the linear absorption coefficient.

The silicon wafers were irradiated at energy densities over a range from 0.7 to 9.5 J/cm^2. Melting of the silicon was evident even at the lowest energy density, which is well above the melting threshold of ≈ 0.13 J/cm^2 for silicon with ArF excimer laser radiation reported elsewhere.[8] Measureable ablation did not occur below a threshold energy density of ≈ 1.3 J/cm^2, which corresponds to a power density of $\approx 7.2\times 10^7$ W/cm^2 for an 18 ns KrF laser pulse duration and to a power density of $\approx 9.3\times 10^7$ W/cm^2 for a 14 ns ArF laser pulse. The effect of background helium pressure on the ablation threshold energy was determined in a similar manner in a different experimental cell. The results verified an ArF excimer laser ablation threshold for silicon on the order of ≈ 1 J/cm^2 or $\approx 7\times 10^7$ W/cm^2 with a buffer gas pressure of 1000 Torr of helium, and indicate that this threshold is essentially constant over the range from 1000 Torr to vacuum.

The threshold determined in our study is nearly a factor of 10 higher than the power density threshold of $\approx 10^7$ W/cm^2 determined by Lubben *et al.* for pulsed laser evaporation of Si under vacuum for film growth using KrF laser radiation.[9] They achieved typical deposition rates of 0.5–1 μm/h on a substrate approximately 3 cm away. These material removal rates are too low to be detected in our study where typical repetition rates were 3–5 Hz and exposure times were on the order of several minutes. Melting of the substrate was observed at even the lowest energy density and some material removal may have occurred, but minimum hole depths of ≈ 10 μm are needed for measurable ablation in our determination.

The rapid increase in the ablation rate at 1.3 J/cm^2, corresponding to intensities of $\approx 7.2\times 10^7$ for KrF and $\approx 9.3\times 10^7$ for ArF, indicates the onset of a new, very effective process for material removal at these intensities. Dabby and Paek[10] presented an analytical model to account for explosive material removal by lasers through the "superheating" of subsurface material. They showed that under certain conditions subsurface temperatures can actually be higher than the surface temperature because the surface is efficiently cooled by evaporation. Temperatures may become high enough to cause subsurface vaporization of material and a large pressure buildup which results in the explosive removal of material near the surface. Due to the high absorption coefficients of silicon at both 193 and 248 nm ($\approx 10^6$ cm^{-1}), however, all the energy is absorbed near the surface and no superheating effects occur at these ultraviolet wavelengths.

Excimer laser ablation of metals has recently been investigated by Poprawe *et al.*[11,12] They characterize three different mechanisms for material removal depending on the incident laser intensity. At power densities sufficient to liquefy the material, but below the vaporization threshold, material is removed at very low rates according to the vapor pressure above the liquid. A dense vapor develops above the surface at laser intensities above the vaporization threshold. Initially ionization due to multiphoton processes rapidly converts the vapor into a plasma. Finally this plasma becomes dense enough so that further absorption is dominated by inverse bremsstrahlung. The energy density in the plasma increases and the pressure waves propagating to the surface become large enough to rapidly expel material from the liquefied zone. These shock waves are called laser supported combustion waves (LSC waves) and are accompanied by pressures of several hundred bar. The result is a rapid increase in material removal rate with increasing laser intensity.

At still higher laser intensities, the plasma becomes so dense that absorption occurs almost entirely in a small region near the top of the plasma causing explosive heating of this region, initiating laser supported detonation waves (LSD waves). This process results in a slower increase in ablation rate with increasing laser intensity due to less efficient coupling of the laser energy to the surface.

We have estimated the surface temperature at the ablation threshold shown in Fig. 6, using the equation developed by Rykalin and Krasulin[13] and obtained values of 3000 and 2700 °C for ArF and KrF at 1.3 J/cm^2. This is in very good agreement with the vaporization temperature of 2477 °C for silicon and indicates the onset of the LSC regime. The pressure in the plasma as determined from the spectral width of the Si II lines is of the same order of magnitude as a typical pressure in the LSC regime, whereas the electron density required to cause the same degree of broadening is about one

order of magnitude above typical electron densities in the LSC regime.[12] This makes it likely that pressure broadening is dominant in our plasma and supports the concept of laser supported combustion waves. With pressures of several hundred bar present in the plasma, it is reasonable to expect the ablation process to be independent of the buffer gas pressure over the range from vacuum to 1000 Torr.

IV. CONCLUSIONS

We have investigated the photoablation of silicon by excimer laser radiation. The interaction of an intense excimer laser beam with single crystal silicon in a He atmosphere has been studied by experimentally determining the silicon ablation rate as a function of pulse energy and spectroscopically analyzing the plasma plume that was formed. Solid material was ablated from the surface of the silicon when the laser energy density at the irradiated spot was more than ≈ 1.3 J/cm^2. Further interaction of the laser energy with the ablated material subsequently caused the ionization of silicon to Si II and Si III and the formation of a Si plasma above the surface. The ablation rate was found to be independent of the laser wavelength at 193 and 248 nm, and the threshold energy density was found to be independent of background pressure over the range from vacuum to 1000 Torr. Pressures of several hundred bar were estimated to be present in the plasma through linewidth measurements. These results are consistent with the mechanism for material removal developed by Poprawe *et al.* for excimer laser ablation of metals.[12] By determining the ablation threshold in a similar manner under realistic processing conditions, safe limits on the intensity of laser radiation to be used during laser-assisted processing can be defined.

ACKNOWLEDGMENTS

Silicon sample material was provided by Texas Instruments. We would like to thank Robert Weikle for his assistance. This work was supported by the Robert A. Welch Foundation.

[1]D. J. Ehrlich and J. Y. Tsao, J. Vac. Sci. Technol. B **1**, 969 (1983).
[2]*Laser Diagnostics and Photochemical Processing for Semiconductor Devices*, Materials Research Society Symposia Proceedings, edited by R. M. Osgood, S. R. J. Brueck, and H. R. Schlossberg (North-Holland, New York, 1983).
[3]G. Koren and J. T. C. Yeh, J. Appl. Phys. **56**, 2120 (1984).
[4]A. R. Striganov and N. S. Sventitskii, *Tables of Spectral Lines of Neutral and Ionized Atoms* (IFI/Plenum, New York, 1968), p. 365.
[5]H. R. Griem, *Spectral Line Broadening by Plasmas* (Academic, New York, 1974).
[6]W. L. Wiese, M. W. Smith, and B. M. Miles, Natl. Stand. Ref. Data Ser. Natl. Bur. Stand. **2**, 73 (1969).
[7]M. von Allen, in *Laser and Electron Beam Processing of Materials*, edited by P. S. Peercy (Academic, New York, 1980), p. 9.
[8]G. Gorodetsky, J. Kanicki, T. Kazyaka, and R. L. Melcher, Appl. Phys. Lett. **46**, 547 (1985).
[9]D. Lubben, S. A. Barnett, K. Suzuki, S. Gorbatkin, and J. E. Greene, J. Vac. Sci. Technol. B **3**, 968 (1985).
[10]F. W. Dabby and U.-C. Paek, IEEE J. Quantum Electron. **QE-8**, 106 (1972).
[11]R. Poprawe, E. Beyer, and G. Herziger, Inst. Phys. Conf. Ser. **72**, 67 (1984).
[12]R. Poprawe, thesis, Institute of Applied Physics, Darmstadt, 1984.
[13]N. N. Rykalin and Y. L. Krasulin, Sov. Phys. Dokl. **10**, 659 (1966).